Human Molecular Genetics, 2009, Vol. 18, No. 16 **3014–3025**
doi:10.1093/hmg/ddp239
Advance Access published on May 18, 2009

Human ISD11 is essential for both iron–sulfur cluster assembly and maintenance of normal cellular iron homeostasis

Yanbo Shi, Manik C. Ghosh, Wing-Hang Tong and Tracey A. Rouault*

National Institute of Child Health and Human Development, Molecular Medicine Program, Bethesda, MD 20892, USA

Received February 12, 2009; Revised May 6, 2009; Accepted May 15, 2009

The LYR family consists of proteins of diverse functions that contain the conserved tripeptide 'LYR' near the N-terminus, and it includes Isd11, which was previously observed to have an important role in iron–sulfur (Fe–S) cluster biogenesis in *Saccharomyces cerevisiae*. Here, we have cloned and characterized human ISD11 and shown that human ISD11 forms a stable complex *in vivo* with the human cysteine desulfurase (ISCS), which generates the inorganic sulfur needed for Fe–S protein biogenesis. Similar to ISCS, we have found that ISD11 localizes to the mitochondrial compartment, as expected, but also to the nucleus of mammalian cells. Using RNA-interference techniques, we have shown that suppression of human ISD11 inactivated mitochondrial and cytosolic aconitases. In addition, ISD11 suppression activated iron-responsive element-binding activity of iron regulatory protein 1, increased protein levels of iron regulatory protein 2, and resulted in abnormal punctate ferric iron accumulations in cells. These results indicate that ISD11 is important in the biogenesis of Fe–S clusters in mammalian cells, and its loss disrupts normal mitochondrial and cytosolic iron homeostasis.

INTRODUCTION

Iron–sulfur (Fe–S) clusters are essential cofactors that facilitate a wide range of cellular processes, including electron transfer processes in oxidative phosphorylation, catalysis of enzymatic reactions in aconitase and dehydratases, facilitation of DNA replication and repair activities, and sensing and regulation of iron levels (1). In eukaryotes, Fe–S proteins are located in multiple compartments, including mitochondria, cytosol and the nucleus. Thus far, more than 20 Fe–S biogenesis proteins have been identified (2–4). Disruptions of this important biological pathway are now recognized as the cause of several human diseases, including Friedreich ataxia, iron-sulfur cluster assembly scaffold protein (ISCU) myopathy and an inherited form of sideroblastic anemia caused by a mutation in GLRX5 (5–7). In each of these diseases, mitochondrial iron overload occurs in conjunction with impaired Fe–S synthesis in the affected tissues.

Regulation of mammalian cellular iron homeostasis is linked to the Fe–S biosynthesis machinery by iron-regulatory protein 1 (IRP1), a bifunctional protein that functions either as a cytosolic aconitase when it contains a [4Fe–4S] cluster, or as an RNA-binding protein that regulates expression of ferritin, transferrin receptor 1 (TfR1), and other proteins when it lacks the Fe–S cluster. In the absence of the Fe–S cluster, apo-IRP1 binds to iron-responsive elements (IREs) in transcripts of several iron metabolism proteins. In addition, a second highly homologous iron-regulatory protein, IRP2, also binds to IREs in cells, but IRP2 undergoes iron-dependent degradation in iron-replete cells and is not an Fe–S protein (8–10). The two IRPs sense cytosolic iron level in different ways, as IRE-binding activity of IRP1 is eliminated by insertion of an Fe–S cluster, whereas IRE binding activity of IRP2 is eliminated by degradation of the protein.

In mammalian cells, Fe–S cluster assembly proteins are found in mitochondria, and also in the cytosolic/nuclear compartments, where isoforms of the cysteine desulfurase, cysteine desulfurase (ISCS), and the scaffold proteins, ISCU and NFU, have been identified. In addition, the cytosolic isoform of ISCU has been shown to be important in the formation of the Fe–S cluster of cytosolic aconitase (11). Recently, Isd11 was identified as a protein that formed a stable complex with Nfs1 in yeast, where it was proposed to function as an adaptor and stabilizer of Nfs1 (12,13). Based on homology, we have identified and cloned the human homologue of Isd11, and investigated its role in human cells.

*To whom correspondence should be addressed. Tel: +1 301 496 6368; Fax: +1 301 402 0078; Email: trou@helix.nih.gov

Here, we report that human ISD11 localizes to both the mitochondria and nuclei of human cells and is required for maintenance of both mitochondrial and extra-mitochondrial Fe–S protein activities and normal mitochondrial and cytosolic iron homeostasis.

RESULTS

Cloning of the human ISD11 homolog

The human expressed sequence tag (EST) database was searched, and analysis of multiple ESTs revealed that only one open reading frame (ORF) was highly homologous to yeast Isd11. Analysis of the ORF predicted a 91-amino acid ORF, and analysis of the ORF with the P-sort program (http://psort.ims.u-tokyo.ac.jp/form2.html) identified potential mitochondrial and nuclear targeting sequences (Fig. 1A).

Endogenous human ISD11 localizes to both mitochondrial and nuclear compartments

To determine the cellular localization of human ISD11 (hISD11), endogenous hISD11 was visualized in HeLa cells by immunofluorescence confocal microscopy using an affinity-purified polyclonal rabbit anti-human ISD11 antibody. The endogenous ISD11 and Tom20 (mitochondria marker) were visualized in interphase HeLa cells using Alexa Fluor 488 conjugated goat anti-rabbit IgG (ISD11; green) and Alexa Fluor 546 conjugated goat anti-mouse (Tom20, red) antibodies, respectively, and nuclei were visualized with DAPI. The subcellular distribution of ISD11 (Fig. 1B) was predominantly in the nuclei and mitochondria, but some ISD11 also appeared to be present in cytosol. When the ISD11 and Tom20 images were merged, colocalization of endogenous ISD11 with Tom20 and DAPI was clearly observed in the mitochondria and nuclei, respectively, as shown by the yellow areas for the mitochondria localization (Fig. 1B) and blue–green area for the nuclear part. The localization of endogenous ISD11 protein was also determined in subcellular fractionation studies, which revealed that a single ISD11 band was present in both the nuclear extract and the mitochondrial fractions (Fig. 1C). Since ISD11 is believed to function in a complex with ISCS, we performed immunohistochemistry of ISCS using an affinity-purified antibody previously described (14) and discovered that endogenous human ISCS was robustly localized to the nucleus (Fig. 1D) in a pattern similar to that of ISD11, with absence of staining in discrete punctate areas of the nucleus that may represent nucleoli. Consistent with previous localization studies in mammalian cells (11,15), cellular fractionation revealed that the cysteine desulfurase, ISCS, and the scaffold protein, ISCU, were also detected in both mitochondrial and nuclear fractions (Fig. 1E) of well-fractionated lysates in which the nuclear extract was not contaminated organellar proteins such as mitochondrial aconitase. Thus, sequence analysis, immunofluorescence and subcellular fractionation experiments supported nuclear and mitochondrial localization of human ISD11, and nuclear localization of its proposed binding partner, ISCS.

Co-immunoprecipitation of ISD11 with ISCS in HeLa cells reveals *in vivo* complex formation

As Isd11 and the cysteine desulfurase, Nfs1, were recently shown to form a complex in *S. cerevisiae* (12,13), we sought evidence that complex formation occurred in mammalian cells. Using antibodies to ISD11 and ISCS, we demonstrated complex formation between endogenous ISD11 and ISCS *in vivo* with co-immunoprecipitation assays (Fig. 2). IgG served as a specificity control for the immunoprecipitation assays (Fig. 2A and B, lane 1). After immunoprecipitation of HeLa cell lysate with anti-ISCS antibody, western blotting showed that ISD11 was present in the eluate in the HeLa cell lysate (Fig. 2A). Conversely, immunoprecipitation using the anti-ISD11 antibody followed by western blot analysis of the eluate using anti-ISCS antibody also demonstrated an association between endogenous ISD11 and ISCS (Fig. 2B). Similar to previous observations that ISD11 forms a tight complex with ISCS in yeast both *in vivo* and *in vitro* (12,13), our studies indicate that the endogenous human ISCS and ISD11 proteins form a complex in human cells.

Bacterial overexpression of human ISD11 and the cytosolic isoform of ISCS facilitates recovery of an active cysteine desulfurase complex

In our previous attempts to over-express the cytosolic form of ISCS in bacteria, we were unable to obtain functional protein because most of the over-expressed protein was sequestered in inclusion bodies. To obtain human ISCS for functional studies, we overexpressed the cytosolic isoform in *Pichia pastoris* (15). Since the bacterially over-expressed cytosolic form of ISCS was mostly misfolded and sequestered within inclusion bodies, we postulated that co-expression with ISD11 might form a complex that would facilitate correct folding and function of ISCS and we co-expressed human ISD11 fused to GST, and human c-ISCS with a myc epitope tag in *Escherichia coli*.

To evaluate the cysteine desulfurase activity of the coexpressed ISD11 and ISCS, we measured enzymatic activity using an assay based on ability of the enzyme to generate hydrogen sulfide (16). The sulfide was detected after converting it to methylene blue in an acidified solution of *N*,*N*′-dimethyl-p-phenylenediamine and $FeCl_3$. After co-overexpression of c-ISCS with GST-tagged ISD11, c-ISCS was present in the soluble fraction of the bacterial lysate. Whereas most of the cISCS expressed in the absence of ISC11 was found in inclusion bodies (data not shown), the cysteine desulfurase activity increased 5-fold in lysates of *E. coli* that co-overexpressed c-ISCS and ISD11, compared with lysates from strains transformed with empty plasmid, ISD11 or c-ISCS alone. Thus, we infer that ISD11 facilitated correct folding of c-ISCS and thereby enhanced the cysteine desulfurase activity recovered from the soluble fraction of bacterial lysates.

ISD11 is required for the biogenesis of human Fe–S proteins

As it has been previously demonstrated that ISD11 is involved in Fe–S cluster biogenesis in yeast (12,13), we assessed the

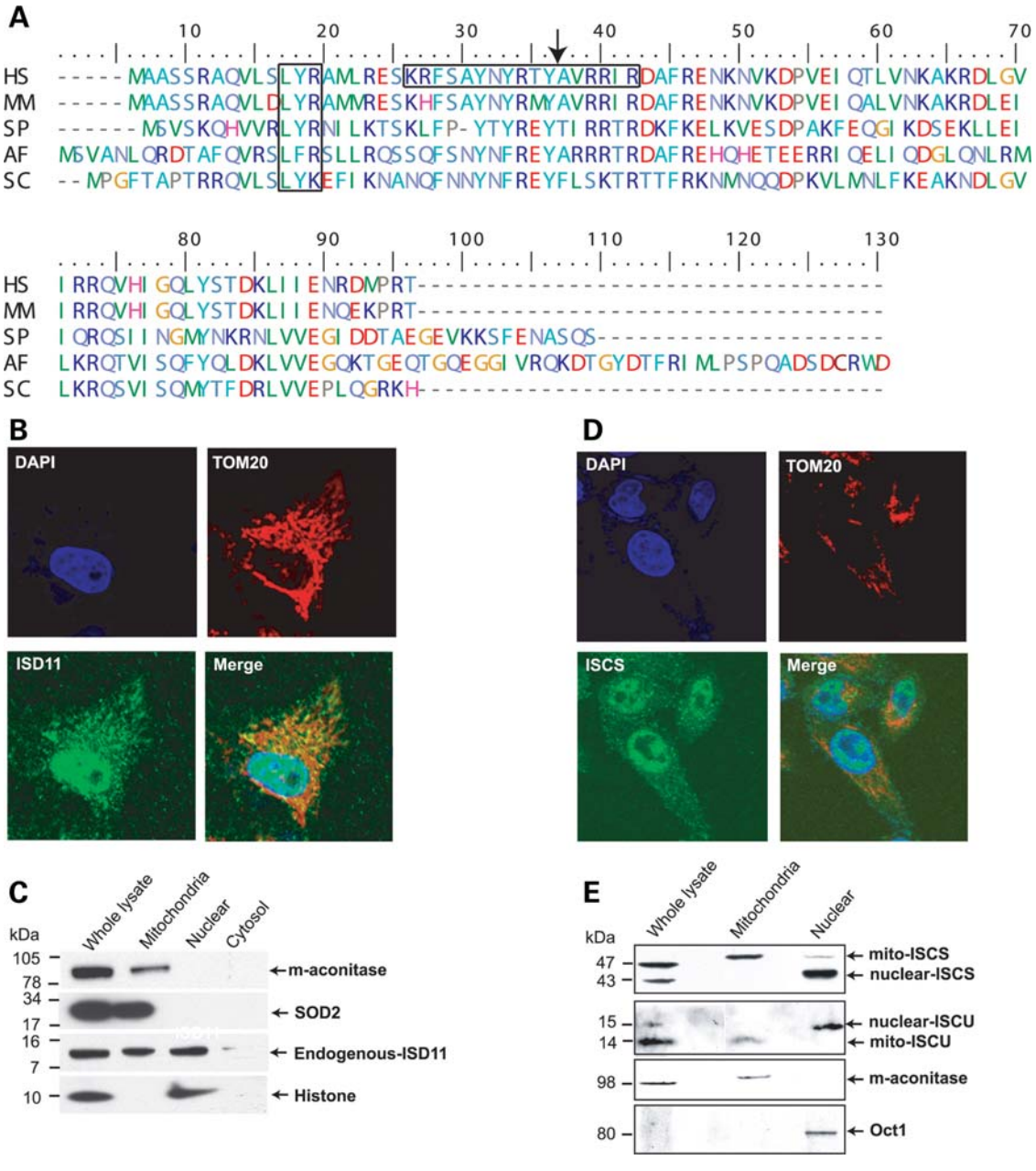

Figure 1. Human ISD11 is localized to both mitochondrial and nuclear compartments. (**A**) An alignment of the human ISD11 amino acid sequence (HS-*Homo sapiens*) compared with sequences of several bacterial and eukaryotic counterparts, including MM (*Mus musculus*), SP (*Schizosaccharomyces pombe*), AF (*Aspergillnus fumigatus*) and SC (*Saccharomyces cerevisiae*). The amino acid sequence of human ISD11 contains a bipartite NLS-like sequence found by the PSORT program (boxed amino acid residues 38–42), and homologies with corresponding regions of several bacterial and eukaryotic homologues are highlighted. In addition, the LYR sequence motif is boxed, and cleavage site of a mitochondrial targeting sequence produced by PSORT is indicated by an inverted arrow. (**B**) Immunofluorescence localization of endogenous ISD11 protein (green) and the mitochondria membrane protein Tom20 (B, red) in HeLa cells stained with the nuclear DAPI stain (blue). The bottom right panel shows the ISD11/Tom20/DAPI merged image. (**C**) Western blot of whole cell lysate and subcellular mitochondrial, cytosolic and nuclear fractions of HeLa cells with SOD2 used as the mitochondrial marker, IRP1 and α-tubulin used as the cytosol markers and histone used as a nuclear marker. Endogenous ISD11 was detected in mitochondrial and nuclear fractions. (**D**) Immunofluorescence localization of endogenous ISCS protein (green) and the mitochondria membrane protein Tom20 (red) in HeLa cells stained with the nuclear DAPI stain (blue). The bottom right panel shows the ISCS/Tom20/DAPI merged image. (**E**) Western blots of HeLa subcellular fractions using m-aconitase as the mitochondrial marker and Oct 1 as the nuclear marker. Endogenous ISCS and ISCU are detected in both mitochondrial and nuclear fractions. Notably, nuclear and mitochondrial isoforms of both ISCS and ISU differ in size, whereas ISD11 has only one size that is detected in nuclear and mitochondrial fractions.

role of human ISD11 in human Fe–S biogenesis by performing ISD11 RNA-interference (RNAi) in HeLa cells and measuring the enzymatic activities of several Fe–S proteins. Three siRNA oligos were designed and used for transfections. RT–PCR analysis of the ISD11 transcript showed that the highest level of inhibition was reached 72 h post-transfection after three successive transfections (data not shown). After three successive RNAi treatments, a >70% reduction of the

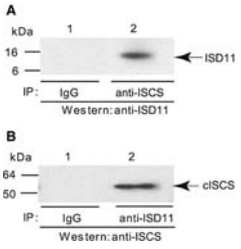

Figure 2. Endogenous ISD11 forms a complex with ISCS *in vivo*. Co-immunoprecipitation of extracts prepared from HeLa cell lysate was performed as described in Materials and Methods. Cell lysates were first immunoprecipitated with anti-ISCS antibody (**A**; Lane 2) or anti-ISD11 antibody (**B**; Lane 2), or IgG as negative control (A and B; Lane 1) followed by western blot analysis using anti-ISD11 (A) or anti-ISCS antibody (B), respectively.

ISD11 mRNA was achieved when compared with the control by quantitative real-time PCR (Fig. 3A). At the protein level, western blot showed that total ISD11 was reduced to less than 30% after three successive transfections (Fig. 3B), and the densitometric quantitative analysis of multiple samples was consistent (Fig. 3C).

To investigate the role of ISD11 in the human Fe–S biosynthesis, a non-denaturing aconitase activity assay was used to monitor Fe–S cluster assembly in the mitochondria and cytosol of HeLa cells. Since both mitochondrial and cytosolic aconitase (IRP1) contain a [4Fe–4S] cluster, and our studies demonstrated that ISD11 formed a complex with ISCS both *in vivo* and *in vitro*, we hypothesized that the silencing of ISD11 would interfere with Fe–S cluster biogenesis through its effect on ISCS function. After four successive ISD11 RNAi treatments, both the mitochondrial and cytosolic aconitase activities were decreased, with a reduction of approximately 50% of m-aco, and >80% of c-aco activities (Fig. 4A). As expected based on many previous studies, the protein levels of c-aconitase (IRP1) were not significantly altered upon depletion of ISD11 as determined by western blotting (Fig. 4B). The strong reduction of the enzyme activities of aconitase (a [4Fe–4S] protein) strongly supports the view that ISD11 functions in both mitochondrial and cytosolic [Fe–S] protein assembly, in agreement with our previous observations of localization of other ISC-assembly proteins (17,18). To confirm the effect on Fe–S proteins in cytosol, we also measured the activity of xanthine oxidase (XO), a [2Fe–2S] enzyme in cytosol. XO activity was also inhibited by nearly 50% in RNAi-treated HeLa cells (Fig. 4C). Taken together, human ISD11 knock-down affects the assembly of both [4Fe–4S] and [2Fe–2S] clusters, either in mitochondria or in cytosol. For comparison, we also investigated if RNAi affected other enzymes that lack a Fe–S cluster. No change was detectable in the activity of lactate dehydrogenase (LDH) (Fig. 4D), pointing to the specificity of action of ISD11 on Fe–S-containing proteins.

Iron-responsive element-binding activities of both IRP1 and IRP2 are activated by ISD11 deficiency

Since complete disassembly of the Fe–S cluster in c-aconitase converts IRP1 to its RNA-binding form, the Fe–S cluster status in the cytosol can also be assessed by monitoring the

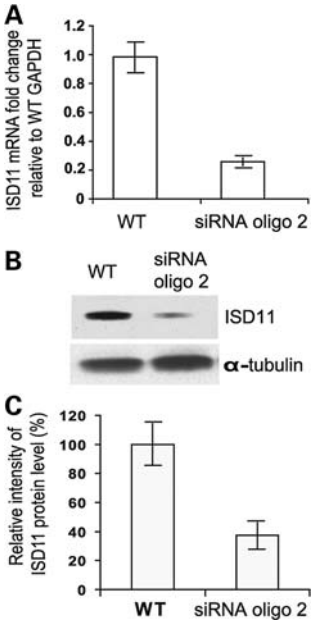

Figure 3. Comparison of protein expression level and mRNA change in ISD11 knock-down HeLa cells and wild-type HeLa cells. Examination of (**A**) mRNA and (**B**) protein expression of ISD11 in wild-type HeLa cells and ISD11 knock-down cells. mRNA and protein expression were assessed as described in Materials and Methods. The western blot panel in (B) represents a typical experiment, whereas (**C**) the densitometry represents the mean ± SD of three experiments.

IRE-binding activity of IRP. To examine whether impairment of [Fe–S] cluster biogenesis affected IRE-binding activity, we prepared a [α-^{32}P]CTP-labeled IRE of ferritin mRNA probe and employed it in an IRP electrophoretic mobility shift assay. Extracts of ISD11-depleted HeLa cells were incubated with the IRE probe, and IRE-binding activity of IRP1 and IRP2 increased (Fig. 4E), even though IRP1 protein levels were unchanged (Fig. 4B), consistent with the possibility that the Fe–S cluster was not synthesized in the absence of ISD11. In addition, levels of IRP2 detected in gel retardation assays appeared to be elevated in ISD11 RNAi-treated samples relative to wild-type cells and negative control samples. To better assess whether IRP2 levels increased in cells in which ISD11 was knocked down, we quantified total IRP2 levels by western blot in cells of WT and ISD11 knock-down cells. An approximately 2.5-fold increase was observed in IRP2 levels in the ISD11 knock-down cells (Fig. 4F), and a statistically significant increase of IRP2 in ISD11 RNAi samples was demonstrated (Fig. 4F), suggesting that cytosol was iron-deficient, since IRP2 levels increase in cells that have cytosolic iron deficiency (9,10).

Misregulation of iron homeostasis in cells depleted of ISD11

Previous studies revealed that iron homeostasis was disturbed in yeast strains with ISD11 mutations (13). To determine whether iron homeostasis was disrupted in human cells with reduced ISD11 levels, direct analysis of the cellular iron

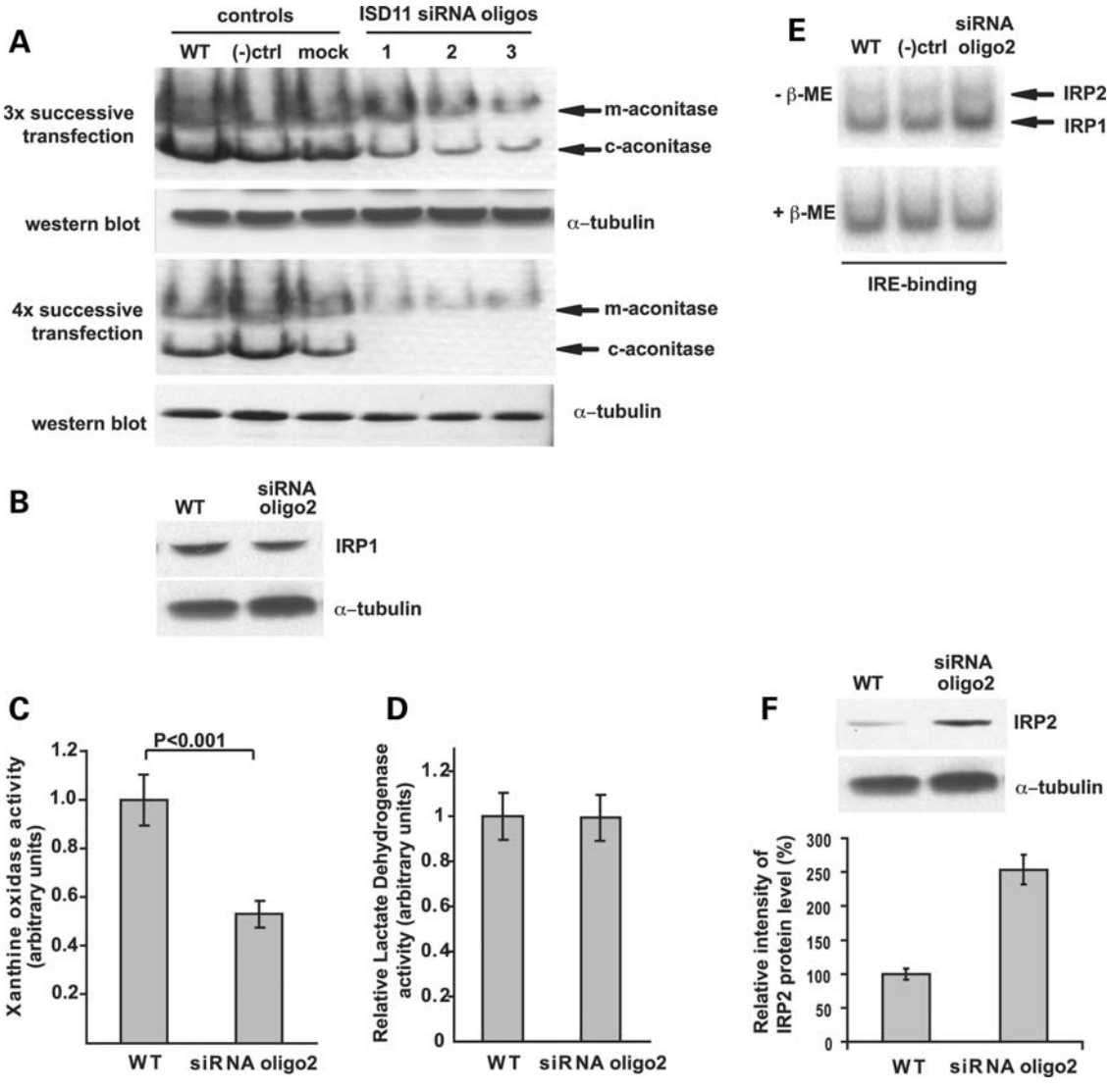

Figure 4. Silencing of ISD11 diminishes mitochondria and cytosolic aconitase activities and activates iron-responsive element (IRE)-binding activity. (**A**) Aconitase activity assay revealed reduced activity of Fe–S cluster enzymes in cells treated with ISD siRNA [WT, wild-type; (−)Ctrl, negative control; Mock, treated with Lipofectamine 2000 reagent; oligo, siRNA of ISD11]. (**B**) Western blots of cells transfected with ISD11 siRNA revealed that (iron-regulatory protein) IRP1 and α-tubulin levels (loading control) did not significantly change. Results shown are representative of four independent experiments. (**C**) Xanthine oxidase activity assay shows obvious decrease in the RNAi-treated cells compared with the untreated wild-type cells. (**D**) Lactate dehydrogenase activity assay shows no change in the RNAi-treated cells compared with the untreated wild-type cells. (**E**) Gel retardation assays of IRPs. Transfected cells were harvested nine days after three times successive transfection and analyzed for total binding activity of IRP1 and IRP2 to ^{32}P-labeled IRE of human ferritin mRNA. Lysates of WT and ISD11 knock-down HeLa cells (10 μg protein/lane) were incubated with ^{32}P-IRE and resolved on a 10% non-denaturing gel. Binding of IREs to IRPs were visualized by autoradiography in the absence of β-mercaptoethanol and quantified using a phosphorimager. Both IRPs have increased IRE-binding activity. (WT, wild type; (−)Ctrl, negative control; oligo2, siRNA of ISD11). IRP1- (bottom band) and IRP2 (up band)-IRE complex. (**F**) Quantitative analysis of IRP2 levels by western blot revealed that IRP2 levels increase in ISD11-depleted cells (top panel) and the result is reproducible (bottom panel).

status including an iron content assay and Perls' diaminobenzidine (DAB) staining were performed. Comparison between all controls and RNAi-treated samples was performed using analysis of variance (ANOVA) followed by two-tail Dunett's test, with a *P*-value of less than 0.05 considered to be significant. The results shown are representative of data from three independent experiments with similar results. Statistical analyses of the data from these three experiments showed that there is no significant difference among wild-type, mock and negative control, since the iron contents [μg/dl (Fe^{2+})] were 51.1 ± 2.58; 48.8 ± 1.03 and 54.87 ± 1.65, respectively. In contrast, the iron contents were 85.43 ± 2.41 for oligo1-treated cells, 154.60 ± 5.02 for oligo2-treated cells and 123.33 ± 5.59 for oligo3-treated cells; these values are significantly different ($P < 0.05$) from those for RNAi oligo-treated cells. The cellular iron content assays showed that total cellular non-heme iron was increased 1.8–3-fold in ISD11-deficient cells compared with the control cells (Fig. 5A), indicating that cellular iron homeostasis was disrupted by ISD11 depletion.

In addition, in the Perls' DAB staining assay, punctate ferric iron staining was shown in cells depleted of ISD11

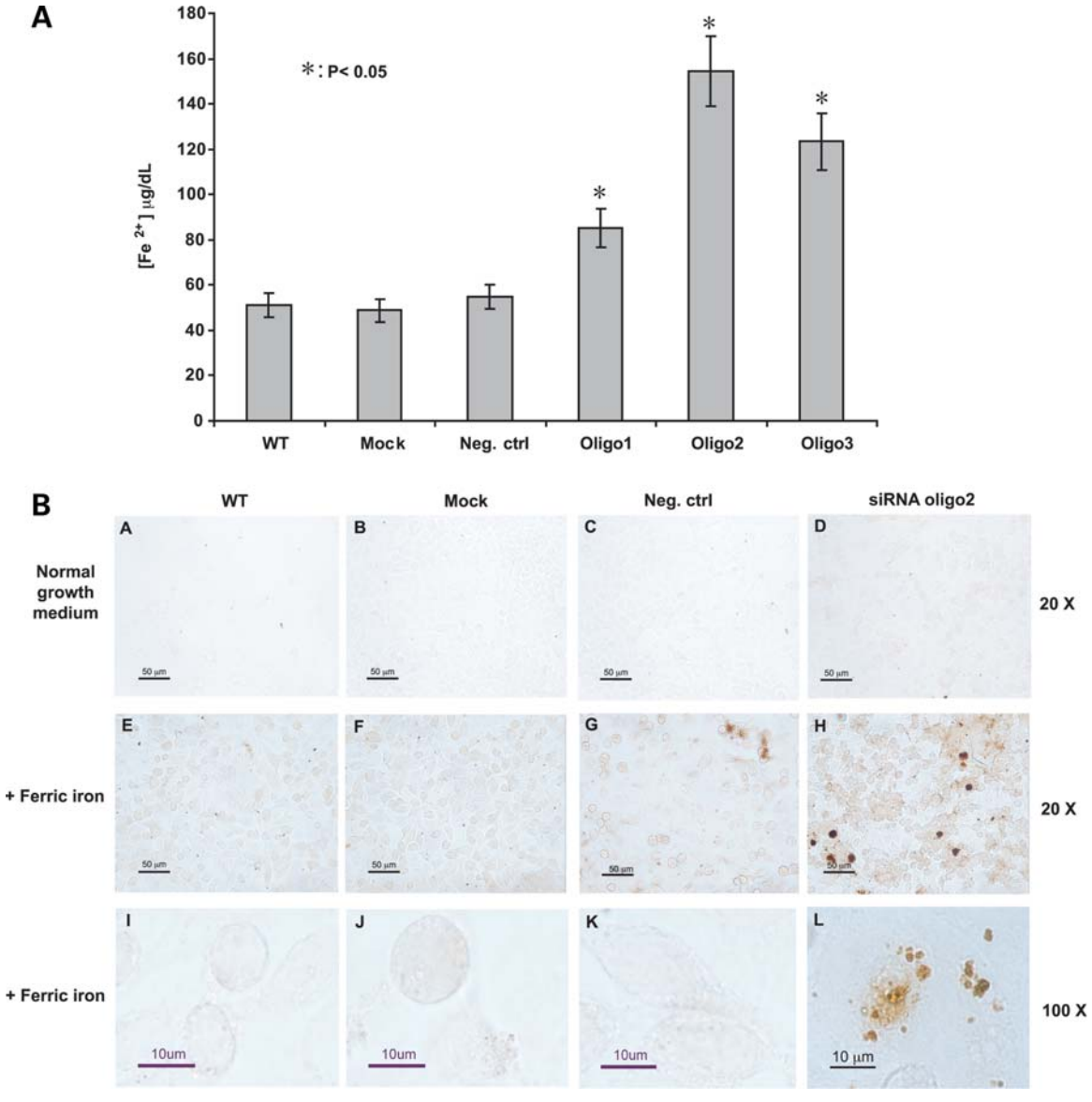

Figure 5. Misregulation of iron homeostasis in cells depleted of ISD11. (**A**) Iron contents assay. Iron contents were determined as described in Materials and Methods, *Y*-axis stands for the value of iron contents in the unit of μg/dl [Fe^{2+}]. Data are mean ± SE ($n = 3$). Analysis of variance (ANOVA) was used for the statistical analysis, with *P*-value is <0.05 considered to be significant. The results shown are representative of data from three independent experiments with similar results. Statistical analyses of the data from these three experiments showed that there is no significant difference among wild-type, mock and negative control, since the iron contents were 51.1 ± 2.58; 48.8 ± 1.03 and 54.87 ± 1.65, respectively. However, the iron contents were 85.43 ± 2.41 for oligo1-treated cells, 154.60 ± 5.02 for oligo2-treated cells and 123.33 ± 5.59 for oligo3-treated cells; these values are significantly different ($P < 0.05$) from those of RNAi oligo-treated cells, as calculated by ANOVA followed by two-tail Dunett's test. (**B**) Perls' diaminobenzidine Ferric iron staining of wild-type cells (**A** and **E**), mock-transfected cells (**B** and **F**), cells transfected with negative control siRNA (**C** and **G**) and cells transfected with ISD11 siRNA (**D** and **H**) in normal or iron-supplemented medium.

(Fig. 5B, D, H and L) but not in control cells (Fig. 5A–C). Furthermore, when the cells were cultured in iron-supplemented medium, iron accumulation was substantially increased in cells transfected with ISD11-siRNA (Fig. 5B, panels H and L) compared with control cells (Fig. 5B, panels E–G and I–K).

As IRE-binding activity of both IRP1 and IRP2 was increased, we studied two target proteins of the IRP-mediated post-transcriptional regulation, ferritin and TfR1 and found that expression of both target transcripts was affected. Both H and L ferritin mRNAs contain a single IRE in their 5′-UTR. Binding of IRPs to these IREs inhibits ferritin translation and thus decreases cytosolic iron storage capacity. In our study, RNAi of hISD11 did not affect ferritin mRNA levels (Fig. 6A, right panel), but the amount of H-ferritin protein in HeLa cells upon ISD11 depletion changed (Fig. 6B, middle panel), with a statistically significant 2-fold decrease (Fig. 6C, right panel), a finding consistent with the increased IRE-binding activity of IRPs (Fig. 4E). In addition, expression of TfR1, a cell surface receptor responsible for the

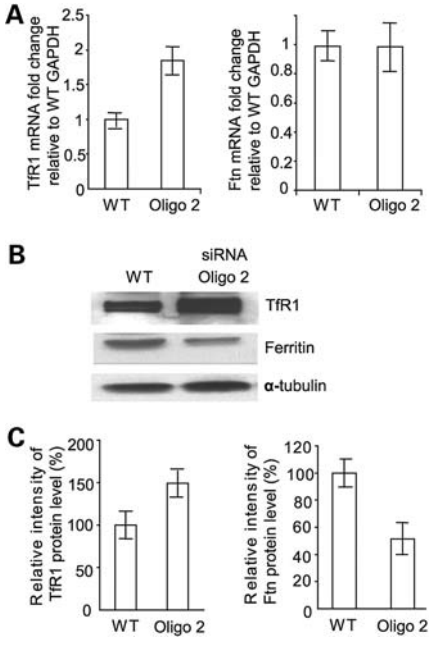

Figure 6. ISD11 knock-down leads to increased TfR1 and decreased ferritin protein levels along with increased TfR1 mRNA level, but no change of ferritin mRNA levels. Comparison of mRNA change and protein expression levels were carried out in ISD11 knock-down HeLa cells and wild-type HeLa cells as described in Materials and Methods. (**A**) ISD11 knock-down cells show increased TfR1 mRNA (left panel), whereas no obvious change of ferritin mRNA was observed (right panel) when compared with wild-type HeLa cells. (**B**) At the protein expression level, TfR1 was increased and ferritin was decreased in the ISD11 knock-down HeLa cells compared with wild-type HeLa cells. The western blot panel in Figure 7B shows a representative experiment. (**C**) shows the mean ± SD total in three experiments.

uptake of iron bound to transferrin (19) increased. Unlike ferritin, the TfR mRNA contains five IREs in its 3′-UTR, and binding of IRPs to these IREs stabilizes the mRNA against degradation, leading to increased TfR mRNA expression and increased TfR1 protein levels (Fig. 6A, left panel and B, top panel) and hence increased transferrin uptake. Thus, all of the above evidence showed that ISD11 silencing caused a cytosolic iron deficiency phenotype, as evidenced by activation of IRE-binding activity of IRP1 and IRP2. Although total cellular iron stores were increased, iron appeared to be sequestered in punctate iron deposits consistent with mitochondrial localization. Thus, ISD11 activity is important for maintenance of cellular iron homeostasis. The subcellular localization of ISD11, other Fe–S biogenesis proteins, and other iron metabolism proteins is summarized in Figure 7.

DISCUSSION

In the present study, we used RNAi technology to evaluate the molecular consequences of depletion of human ISD11, the homologue of yeast Isd11, which was previously shown to facilitate activity of the yeast cysteine desulfurase, Nfs1. Significant decreases of hISD11 content resulted in >3-fold reduced activities of the Fe–S proteins mitochondrial aconitase, cytosolic aconitase and XO, and increased IRE-binding activity of cytosolic protein IRP1, which clearly indicated the absence of its Fe–S cluster. These results indicate that human ISD11 plays an essential role in the maintenance of [Fe–S] protein activities, as was previously observed in yeast (12,13). Although the precise role of ISD11 function in the biogenesis of [Fe–S] proteins has not yet been fully elucidated, studies in yeast suggested that Isd11 stabilizes the yeast cysteine desulfurase, Nfs1 (12,13), and our studies indicated that hISD11 forms a stable complex with hISCS.

Analysis of the subcellular localization of human ISD11 revealed that human ISD11 was found in abundance in mitochondria, as expected, but also in the nuclear compartment, unlike in yeast, where Isd11 was found only in mitochondria (12,13). Both ISCS and ISD11 were readily detected in the nuclear compartment of human cells by fractionation and immunohistochemistry, consistent with the observation that endogenous ISD11 forms a complex with ISCS. Although ISD11 could potentially traffic to the nucleus by virtue of its association with human ISCS, which contains a nuclear localization signal, sequence alignments revealed that ISD11 itself contains a conserved nuclear localization signal, which may enable ISD11 to localize to the nucleus independent of ISCS. These results fit with subcellular localization data on other members of the human ISC assembly machinery, including hISCU, hISCS and hNFU, each of which generate two distinct isoforms that target to either the mitochondria or cytosolic/nuclear compartments because they either contain or lack the mitochondrial signal peptide. Previous results are further confirmed by detection of ISCU in the nuclear fraction of Hela cells in this paper. Through alternative translation initiation or alternative splicing of mRNA, the ISC assembly proteins hISCU, hISCS and hNFU have been previously found in cytosol and/or nucleus, which led to the suggestion that the mitochondrial ISC machinery was duplicated in the cytosolic/nuclear compartment of human cells to synthesize Fe–S clusters for extra-mitochondrial Fe–S proteins (4,20). Although we did not find evidence for alternative splicing of ISD11, our results demonstrate that endogenous ISD11 can target both the mitochondrial and nuclear compartments of human cells.

Even though Isd11 was not found in the nuclear/cytosolic compartment of yeast, studies on Isd11 in yeast have shown that it forms a complex with Nfs1 that enhances cysteine desulfurase activity of Nfs1, which is both a mitochondrial and nuclear protein in yeast. Cytosolic/nuclear forms of ISCS were found in both yeast and humans (14,17,18,21), although nuclear localization was faint in human cells (22). Several studies concluded that nuclear Nfs1 of yeast was required for cell viability (23) and for thiolation of tRNAs in the nucleus, similar to bacterial IscS (24–26), but not for Fe–S cluster assembly (22). Because we have not identified an alternative transcript that encodes the nuclear form of ISD11, we cannot specifically target the nuclear pool of ISD11 with RNAi, and we cannot directly evaluate the role of ISD11 in nuclear/cytosolic Fe–S biogenesis, as was done previously with specific targeting of the cytosolic/nuclear ISCU isoform (11).

There are several possible roles for ISD11 in the nucleus. First, it may be involved in Fe–S cluster assembly in the nucleus, similar to its role in the mitochondria. A [4Fe–4S] cluster containing protein called Ntg2p, a yeast homologue

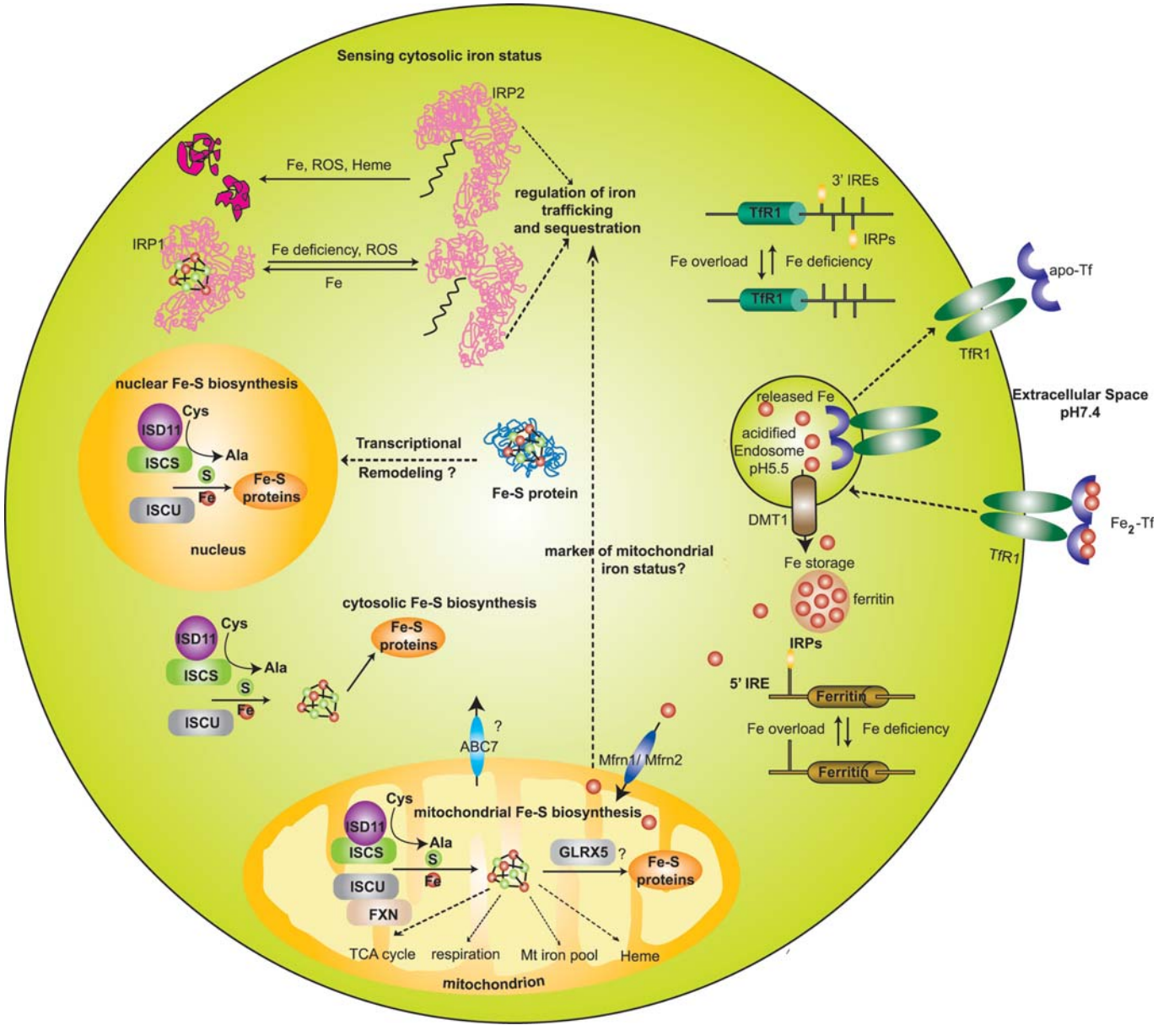

Figure 7. Proposed working model for human ISD11 in both Fe–S cluster biogenesis and mammalian iron homeostasis. Extracellular diferric transferrin (Tf–Fe_2) binds to the dimeric transferrin receptor (TfR) and is internalized by receptor-mediated endocytosis. Iron is then transported from endosomes into the cytosol by the divalent metal transporter-1 (DMT1). In the cytosol of mammalian cells, iron status is registered by the assembly and disassembly of a [4Fe–4S] cluster in iron-regulatory protein-1 and the iron-dependent degradation of IRP2, which reflects intracellular iron levels. IRPs regulate the levels of the TfR and the iron storage protein ferritin, along with DMT1 and the iron exporter ferroportin, by binding to iron-responsive elements in their transcripts. In the mitochondria, the citric acid cycle, respiratory complexes and heme biosynthesis are all dependent on iron availability and Fe–S cluster biogenesis. Mitochondrial Fe–S protein biosynthesis requires the cysteine desulfurase ISCS, the scaffold protein ISCU and ISD11, in addition to other proteins such as frataxin and GLRX5. We have previously shown that Fe–S biogenesis takes place in the cytosolic compartment of mammalian cells, and here we show that ISD11, ISCS and ISCU are all present in the nucleus, where they likely facilitate nuclear Fe–S biogenesis.

of endonuclease III, has been shown to be present in the eukaryotic nucleus (27), and the DNA repair helicases XPD and FancJ also have been shown to contain essential [Fe–S] clusters in their active sites (28,29). Mutations in patients with trichothiodystrophy and Fanconi anemia disrupt the Fe–S clusters of XPD and FancJ and thereby abolish helicase activity. Thus, much evidence implies that nuclear Fe–S proteins are important for maintenance of the integrity of the mammalian genome, and we suggest that nuclear ISD11 likely functions as a partner or stabilizer of ISCS in the biogenesis of nuclear localized [Fe–S] proteins such as Ntg2p, XPD and FancJ. As several other Fe–S biogenesis genes are now recognized as human disease genes (4), it is possible that ISD11, which localizes to human chromosome 6p25.1 and traffic to the nucleus, will also prove to be a cause of human disease.

Our co-immunoprecipation results with HeLa cell lysates demonstrated that a tight complex was formed between

endogenous ISD11 and ISCS, and our biochemical assays support that ISD11–ISCS complexes have cysteine desulfurase activity. Previously, it was thought that Nfs1 alone could liberate sulfur from cysteine, since the purified recombinant protein exhibited the enzymatic activity as a cysteine desulfurase and released sulfide *in vitro* under reducing conditions (21). However, the reaction *in vivo* is different, as no free sulfide is generated during Fe–S assembly *in vivo*. Recent studies in yeast have shown that without functional Isd11, Fe–S clusters cannot be formed on the scaffold Isu and subsequently transferred to target apoproteins *in vivo* (12,13). In this present study, the desulfurase activity assay based on a bacterially co-overexpressed GST-tagged version of ISD11 and myc-tagged c-ISCS showed higher activity, whereas expression of cISCS alone showed poor activity. Our data support that ISD11 acts as an adaptor of ISCS by forming a tight complex that helps ISCS to fulfill the cysteine desulfurase function in the Fe–S cluster biosynthesis either in mitochondria or in the nuclear/cytosolic compartment of human cells.

An important finding in the present study is that depletion of ISD11 disrupted not only Fe–S cluster biogenesis, but also iron-sensing and regulation in human cells. In mammalian cells, iron uptake and metabolism are mainly regulated by IRP1 and IRP2 through post-transcriptional regulation. In the present study, we demonstrated that siRNA-mediated silencing of ISD11 resulted in increased IRE-binding activity of IRP1 and IRP2 together with increased IRP2 protein levels (Fig. 4F) and an unusual pattern of iron accumulation in cellular punctate structures that likely represent mitochondria (Fig. 5B, L). As indicated by western blot and band-shift assay, the strongly decreased ferritin protein levels are consistent with translational repression caused by increased IRP-binding. In contrast to ferritin, IRP-binding to the 3′-UTR of IRE stabilizes and promotes TfR mRNA translation. As a result, the cellular TfR protein levels were strongly increased because of the ISD11 depletion, but most iron appeared to accumulate in mitochondria, whereas cytosolic iron was functionally depleted. Taken together, these results point out a role of ISD11 in the synthesis of both mitochondrial and cytosolic/nuclear Fe–S proteins. Absence of ISD11 resulted in cytosolic iron depletion, as evidenced by increased IRP2 levels, and mitochondrial iron overload, as evidenced by iron staining. These results suggest that mitochondrial iron homeostasis is disrupted when Fe–S cluster biogenesis is impaired, as has previously been observed for other Fe–S cluster biogenesis proteins including frataxin, Nfs1, ISCU and numerous others (4). The identification of human ISD11 as an important component of [Fe–S] protein biogenesis may help to achieve deeper insights into [Fe–S] assembly and cellular iron homeostasis.

MATERIALS AND METHODS

Cloning, expression and purification of human ISD11

A clone that contained the putative human ISD11 sequence was obtained from the human EST database and purchased from ATCC (IMAGE 3898393) followed by sequencing, then was used as the PCR template to clone mature human ISD11 into pGEX4T-3 (Sigma) to generate a ISD11/GST fusion protein. Two primers [mISD_F_EcoRI, CCG*GAATT C*CATGGCTGTCAGGAG, and mISD_R_XhoI, AGT*CT CGAG*CTAGGTCCTGGGCAT (italicized portions of sequences indicate restriction sites)] were used in the PCR to generate a fusion of amino acids 37–96 of ISD11 to GST. All of the plasmid constructs were confirmed by DNA sequencing. For purification of hISD11, the pGEX4T -3/hISD11 plasmid was transformed into *E. coli* BL21(DE3) plyss cells. Cells were grown at 30°C in 1L cultures of 2YT broth containing 100 μg/mL ampicillin and induced at OD_{600nm} with 800 μM isopropyl-β-D-thiogalactoside (IPTG) for another 3 h, after they were harvested by centrifugation at 10 000*g*, lysed with the one-shot cell disrupter (Cell Disruption System, St-Laurent, Quebec, Canada), and centrifuged at 30 000*g* for 30 min. Final purification of pGEX4T-3/hISD11 was achieved by chromatography on a GST column (GE Healthcare), and eluted with 50 mM Tris–HCl, 10 mM GSH. For coexpression of human cytosolic ISCS (pT 7-hNIFS*c*-myc) (14) and ISD11 in *E. coli*, corresponding plasmids were co-transformed into BL21(DE3) plyss cells. Cells were grown and harvested under the conditions stated above.

Antibody production

The rabbit polyclonal antibody was raised against antigenic protein of human ISD11 which was cleaved from a GST fusion protein generated from pGEX 4T-3/hISD11 with thrombin. Antiserum was generated in New Zealand white rabbits by Covance Laboratories Inc. (Vienna, VA, USA). Antibody to human ISCU and ISCS were generated as described previously (14,17). Immunoaffinity purification of antisera were carried out using purified ISD11, MAP peptides of ISCU and ISCS immobilized on CNBr-activated Sepharose 4B (Pharmacia) for immunohistochemistry, and Melon™ Gel IgG Spin Purification Kit (Thermo scientific) for ISCS antibody for immunoprecipitation.

Cysteine desulfurase activities assay

BL21 (DE3) *E. coli* cells co-transfected with c-ISCS and ISD11 were lysed in lysis buffer (25 mM Tris–HCl, pH 8.0, 100 mM NaCl, 2.5 μg/ml aprotinin, 5 μg/ml leupeptin, 0.4 mM phenylmethylsulfonyl fluoride, and 5 mM benzamidine). After cells were broken with cell disruptor, the lysate was centrifuged at 30 000*g* for 30 min and the supernatants containing over-expressed c-ISCS and ISD11 were filtered through a 0.22 μm filter before use in further studies.

L-Cysteine desulfurase activity of cISCS/ISD11 was assayed at 37°C and quantified by the methylene blue method as described (16). Briefly, 160 μl of reaction mixture contained 25 mM Tris–HCl, pH 7.4, 100 mM NaCl, 1 mg total protein of cell lysate, 10 μM pyridoxal 5′-phosphate (Sigma), 1 mM dithiothreitol (Sigma). The reactions were initiated by the addition of L-cysteine (Sigma) and incubated for 10 min at 37°C before the reactions were stopped by the addition of 20 μl of 20 mM *N*,*N*-dimethyl-*p*-phenylenediamine in 7.2 M HCl. Methylene blue was formed by the addition of 20 μl of 30 mM $FeCl_3$

in 1.2 M HCl. After 30 min incubation, samples were centrifuged for 10 min at 16 000*g* and the supernatant was assayed by measuring the absorbance at 670 nM. The standard curve was calibrated with sodium sulfide (0–100 μM). One unit of enzyme activity corresponds to 1.0 μmol of substrate converted per minute.

Cell cultures, lysates and subcellular fractionation

HeLa cells were grown in Dulbecco's modified Eagle's medium (DMEM)-complete medium [DMEM medium supplemented with 10% fetal calf serum (FCS), 10% U/ml Penicillin–Streptomycin (Gibco) and 2 mM L-glutamine (Gibco)] in a humidified incubator at 5% CO_2. Treatments with the iron chelator, deferoxamine mesylate (DFO, Sigma) or ferric ammonium citrate (FAC, Fisher Scientific) were performed by incubating cells for 16 h in DMEM-complete medium with 50 μM DFO or 100 μM FAC, then washed and incubated in DMEM-complete medium for up to 24 h. Triton lysates were prepared as previously described with addition of 2 mM citrate. Subcellular fractions were prepared as previously described (17).

RNA-interference assays

The control siRNA was the non-targeting siRNA (Qiagen, MD, USA). siRNAs against human ISD11 were purchased from Qiagen. The target sequences are: ISD siRNA oligo1, CAA GCG TTT CAG CGC CTA CAA; oligo2, AAG AGA GAC CTT GGA GTA ATT; Oligo3, GCT GGA GTT CGT TCA GAA TAG. For RNA-interference experiments, HeLa cells were cultured in DMEM with 10% v/v fetal bovine serum and transfected at 30%–50% confluency with 100 nM siRNA using Lipofectamine 2000 (Invitrogen) every 72 h for 3–9 days. The cells were subsequently harvested and used for further studies.

Enzymatic activity assays

Aconitase activity assay. Aconitase activity gels are composed of a separating gel containing 8% acrylamide, 132 mM Tris base, 132 mM borate, 3.6 mM citrate and a stacking gel containing 4% acrylamide, 37 mM Tris base, 67 mM borate, 3.6 mM citrate. The running buffer contains 25 mM Tris pH 8.3, 192 mM glycine and 3.6 mM citrate. Samples contain cell lysates (100 μg whole protein), 25 mM Tris–HCl, pH 8.0, 10% glycerol and 0.025% bromophenol blue. Electrophoresis was carried out at 180 V at 4°C. Aconitase activities were assayed by incubating the gel in the dark at 37°C in 100 mM Tris (pH 8.0), 1 mM NADP, 2.5 mM *cis*-aconitic acid, 5 mM $MgCl_2$, 1.2 mM MTT, 0.3 mM phenazine methosulfate and 5 U/ml isocitrate dehydrogenase, and quantitation was performed using NIH Image software (ImageJ 1.34s; http://rsb.info.nih.gov/ij) as described previously (11).

Lactate dehydrogenase assay

LDH activity was assessed according to the manufacturer's instructions for both ISD11 RNAi cells and wild-type cells using Sigma Diagnostics' Lactate Dehydrogenase Kit (Product No. TOX-7). Hundred micrograms of whole protein of each sample were used for the assay, an ELISA spectrophotometer system (Fisher Scientific) was used for data acquisition.

RNA mobility shift assays

Gel-retardation assays were performed as described (30) with the following modifications: a 8% acrylamide/TBE gel, pre-run at 200 V for >30 min, and run at 200 V for 3.5 h at room temperature. Cell lysates were prepared in lysis buffer consisting of 10 mM HEPES (pH 7.2), 3 mM $MgCl_2$, 40 mM KCl, 5% glycerol, 0.2% Nonidet P-40, 5 mM dithiothreitol (DTT), 1 mM AEBSF, 10 mg/ml Leupeptin and CompleteTM EDTA-free protease inhibitor cocktail (Roche Applied Science, IN, USA). Equal amounts of about 10 mg of total protein were added to a final volume of 12.5 μl buffer containing 25 mM Tris–HCl (pH 7.5) and 40 mM KCl with or without 2% β-ME, which activates IRP1 *in vitro*. The samples were incubated for 5 min at room temperature (RT) with 12.5 μl of a reaction cocktail containing 20% glycerol, 0.2 U/ml Super Rase-In (Ambion, TX, USA), 0.6 mg/ml yeast tRNA, 5 mM DTT and 20 nM ^{32}P-labeled IRE from the human ferritin H-chain gene in 25 mM Tris–HCl (pH 7.5) and 40 mM KCl. A measure of 20 μl of this reaction mixture was loaded onto a 10% acrylamide/TBE gel, which was run at 200 V for 3.5 h, and then the gel was fixed, dried and exposed for autoradiography.

Quantitative real-time reverse transcriptase–polymerase chain reaction

Total RNA was extracted from HeLa cells using an RNeasy mini kit (Qiagen) according to the manufacturer's instructions, and the quality of RNA (i.e. $A_{260/280} > 1.8$) was confirmed. The determination of mRNA by qRT–PCR was carried out using total RNA (1 μg) as a template and poly (dT) as a primer for cDNA synthesis by SuperScript II reverse transcriptase (Invitrogen). The mRNA levels of ISD11, TfR1 and ferritin were determined by quantitative real-time PCR using SYBR GreenER qPCR supermix (Invitrogen) and an ABI PRISM 7900HT Sequence Detection System.

A typical reaction mixture contained 25 μl of Platinum SYBR Green qPCR SuperMix-UDG, 1 μl of both forward primer (10 μM) and reverse primer (10 μM), 1 μl ROX Reference Dye, cDNA generated from 1 μg of total RNA, supplemented with DEPC-treated water to obtain a reaction mixture with a final volume of 50 μl. The standard cycling program were: 50°C for 2 min; 95°C for 2 min; 40 cycles of 95°C for 15 s, 60°C for 30 s and 70°C for 15 s. The resulting products were analyzed on an agarose gel stained with ethidium bromide (data now shown). The primers used are as follows: Human ISD forward (nucleotides 172–193), 5′-AAAGCCAAGAGAGACCTTGGA-3′, and reverse (nucleotides 276–256), 5′-CTAGGTCCTGGGCATGTCT C-3′; Human Transferrin receptor 1 forward, 5′-CTGGAGA CTTTGGATCGGTTGGTG-3′; and reverse, 5′-CA GTGGCTGGCAGAAACCTTG-3′; Human Ferritin forward: 5′-AGCTCCCAGATTCGTCAGAA-3′; and reverse, 5′-A TCATCGCGGTCGAAATAGA-3′; the primer sequences for

internal control glyceraldehyde-3-phosphate dehydrogenase (GAPDH) forward primer, 5′-TGCACCACCAACTGCTTAGC-3′; reverse primer, 5′-GGCATGGACTGTGGTCATGAG-3′.

Western blot analysis

The protein concentration was determined by the Bradford method (Pierce Chemical Co., Rockford, IL, USA) with bovine serum albumin (Pierce Chemical Co.) as the standard. Western blot analysis was carried out as described previously (17). The primary antibody used in the western blot analysis was polyclonal anti-human ISD11 antibody (1:500 dilution) raised in rabbits (Covance) against mature overexpressed ISD protein obtained from the GST column after cleavage with thrombin (Sigma–Aldrich). Antibodies to human IRP2 were described previously (30). Antibody to m-aconitase was raised against peptide YDLLEKNINIVRKRLNR. IRP1 antibody was polyclonal raised from rabbit. L-Ferritin antibody (1:5000) was a generous gift from Dr Esther G. Meyron-Holtz. α-Tubulin antibody was (1:5000, Sigma). Transferrin receptor1 (TfR1) antibody was purchased from Zymed (1:5000; San Francisco, CA, USA), Histone H4 (1:2000; Upstate, CA, USA), mouse monoclonal α-Oct-1 (Calbiochem) and Sheep polyclonal α -manganese superoxide dismutase (α-Mn-SOD) (Calbiochem), ISCU (1:500), ISCS (1:500). The intensities of the western blot bands were quantified by program ImageJ (http://rsb.info.nih.gov/ij/).

Iron staining

Transfected cells treated with or without 100 mg/ml FAC for 16 h. Cells were fixed and stained in 4% formalin and Perls' solution (1%) $K_4Fe(CN)_6$ and 1% HCl for 30 min at room temperature. After rinsing in PBS for three times, cells were incubated with 0.75 mg/ml DAB (Sigma, D5905), 0.07% H_2O_2 in 1 M Tris (pH 7.5) for 60 min. The reaction was quenched by rinsing in PBS.

Fluorescent confocal microscopy (detection of endogenous ISD11 and ISCS)

Subcellular localization of endogenous ISD11 was visualized by fluorescent confocal microscopy. Cultured HeLa cells were washed four times in DMEM, fixed with freshly prepared 4% paraformaldehyde (20 min at room temperature), and permeabilized with 0.1% Triton X-100 in PBS (15 min at room temperature). Non-specific binding of the antibodies was blocked with normal goat serum (NGS, 10%, Zymed Laboratories, Inc. Cat. 01-3201) and albumin from chicken egg white (OVA, 2%. Sigma, Cat. A5503) at room temperature for 15 min before incubation with the anti-ISD11 antibody (1:500 dilution) and monoclonal anti-Tom20 antibody (1:500 dilution; Santa Cruz Biotechnology, Cat. SC-17764) at room temperature for 45 min, followed by Alexa Fluor 546 conjugated goat anti-mouse (1:400 dilution; Molecular Probes) or Alexa Fluor 488 conjugated goat anti-rabbit IgG (Molecular Probes). Nuclei were also stained with DAPI (Vector Laboratories). Laser confocal scanning images were captured using Zeiss TV200 inverted microscope. The localizations of ISD11 and Tom20 in cells were visualized. Subcellular localization of ISCS (1:250 dilution) was performed with antibody to ISCS as described previously (14), after affinity-purification using MAP peptide (RSRKKHLITTQTEHK) and DAPI and Tom 20 colocalization was performed as described above.

Cell lysis and fractionation

For HeLa Triton lysates, cells were washed with ice-cold PBS and lysed in Triton X-100 Lysis buffer (17). For subcellular fractionation, cell pellets were suspended in digitonin lysis buffer (0.1% digitonin, 210 mM mannitol, 70 mM sucrose, 4 mM HEPES pH 7.2, 1 mM AEBSF, Roche mini cocktail). The lysates were centrifuged at 900*g* for 10 min at 4°C. The supernatants were centrifuged at 14 000*g* for 10 min for 4°C, and the final supernatants were considered as the cytosolic fraction. The pellets from the above lysates were washed and lysed with Triton X-100 lysis buffer and clarified by centrifugation at 16 000*g* for 10 min. The supernatant was considered as the membrane organelle fraction, the pellet containing nuclei was lysed with NER buffer (NE-PER Nuclear and Cytoplasmic Exraction Reagents, Pierce), and the supernatant of the nuclear lysate was clarified by centrifugation at 16 000*g* for 10 min at 4°C.

Co-immunoprecipitation and western blotting

To analyze the association of endogenous ISD11 with ISCS in cells, HeLa cell lysates (1 mg) were immunoprecipitated with 10 μg anti-ISD11 antibody or 10 μg anti-ISCS antibody, followed by western blot analysis using anti-ISCS antibody or anti-ISD11 antibody, respectively. Human IgG was used for negative control samples. ProFound™ mammalian co-immunoprecipitation kit (Pierce, Cat. 23605) was used according to the manufacturer's instruction. For western blot analysis, samples were separated by sodium dodecyl sulfate–polyacrylamide gels and transferred to nitrocellulose, blots were incubated in antibody diluted in blocking buffer (5% non-fat dry milk, 1× TBST) overnight at 4°C. Horseradish peroxidase-conjugated secondary antibodies were detected by an ECL system (Pierce). Band intensities were evaluated using NIH IMAGE Software (ImageJ 1.34s; http://rsb.info.nih.gov/ij).

Statistical analysis

All data excepted for iron content measurements are expressed as means ± SEM. Statistical analysis was performed using unpaired two-tailed Student's *t*-test, with *P*-values <0.05 considered to be significant. In terms of iron content measurement, ANOVA followed by two-tail Dunett's test was used for statistical analysis, with *P*-value <0.05 considered significant.

ACKNOWLEDGEMENTS

The authors would like to thank our colleagues in our laboratory for helpful discussion and Dr George Patterson and Dr Suh-Yeong Jeong for help with confocal microscopy,

Dr Deliang Zhang for valuable suggestions, Dr Rafael Mattera for help with ANOVA statistical analysis.

Conflict of Interest statement. We declare no conflicts of interest.

FUNDING

This work was supported by the Intramural Program of National Institute of Child Health and Human Development.

REFERENCES

1. Beinert, H., Holm, R.H. and Munck, E. (1997) Iron–sulfur clusters: nature's modular, multipurpose structures. *Science*, **277**, 653–659.
2. Johnson, D.C., Dean, D.R., Smith, A.D. and Johnson, M.K. (2005) Structure, function, and formation of biological iron–sulfur clusters. *Annu. Rev. Biochem.*, **74**, 247–281.
3. Lill, R. and Muhlenhoff, U. (2008) Maturation of iron–sulfur proteins in eukaryotes: mechanisms, connected processes, and diseases. *Annu. Rev. Biochem.*, **77**, 669–700.
4. Rouault, T.A. and Tong, W.H. (2008) Iron–sulfur cluster biogenesis and human disease. *Trends Genet.*, **24**, 398–407.
5. Camaschella, C., Campanella, A., De Falco, L., Boschetto, L., Merlini, R., Silvestri, L., Levi, S. and Iolascon, A. (2007) The human counterpart of zebrafish shiraz shows sideroblastic-like microcytic anemia and iron overload. *Blood*, **110**, 1353–1358.
6. Mochel, F., Knight, M.A., Tong, W.H., Hernandez, D., Ayyad, K., Taivassalo, T., Andersen, P.M., Singleton, A., Rouault, T.A., Fischbeck, K.H. *et al.* (2008) Splice mutation in the iron–sulfur cluster scaffold protein ISCU causes myopathy with exercise intolerance. *Am. J. Hum. Genet.*, **82**, 652–660.
7. Olsson, A., Lind, L., Thornell, L.E. and Holmberg, M. (2008) Myopathy with lactic acidosis is linked to chromosome 12q23.3-24.11 and caused by an intron mutation in the ISCU gene resulting in a splicing defect. *Hum. Mol. Genet.*, **17**, 1666–1672.
8. Pantopoulos, K. (2004) Iron metabolism and the IRE/IRP regulatory system: an update. *Ann. NY Acad. Sci.*, **1012**, 1–13.
9. Rouault, T.A. (2006) The role of iron regulatory proteins in mammalian iron homeostasis and disease. *Nat. Chem. Biol.*, **2**, 406–414.
10. Wallander, M.L., Leibold, E.A. and Eisenstein, R.S. (2006) Molecular control of vertebrate iron homeostasis by iron regulatory proteins. *Biochim. Biophys. Acta*, **1763**, 668–689.
11. Tong, W.H. and Rouault, T.A. (2006) Functions of mitochondrial ISCU and cytosolic ISCU in mammalian iron–sulfur cluster biogenesis and iron homeostasis. *Cell Metab.*, **3**, 199–210.
12. Adam, A.C., Bornhovd, C., Prokisch, H., Neupert, W. and Hell, K. (2006) The Nfs1 interacting protein Isd11 has an essential role in Fe/S cluster biogenesis in mitochondria. *EMBO J.*, **25**, 174–183.
13. Wiedemann, N., Urzica, E., Guiard, B., Muller, H., Lohaus, C., Meyer, H.E., Ryan, M.T., Meisinger, C., Muhlenhoff, U., Lill, R. *et al.* (2006) Essential role of Isd11 in mitochondrial iron–sulfur cluster synthesis on Isu scaffold proteins. *EMBO J.*, **25**, 184–195.
14. Land, T. and Rouault, T.A. (1998) Targeting of a human iron–sulfur cluster assembly enzyme, nifs, to different subcellular compartments is regulated through alternative AUG utilization. *Mol. Cell.*, **2**, 807–815.
15. Li, K., Tong, W.H., Hughes, R.M. and Rouault, T.A. (2006) Roles of the mammalian cytosolic cysteine desulfurase, ISCS, and scaffold protein, ISCU, in iron–sulfur cluster assembly. *J. Biol. Chem.*, **281**, 12344–12351.
16. Flint, D.H., Tuminello, J.F. and Miller, T.J. (1996) Studies on the synthesis of the Fe-S cluster of dihydroxy-acid dehydratase in *Escherichia coli* crude extract. Isolation of O-acetylserine sulfhydrylases A and B and beta-cystathionase based on their ability to mobilize sulfur from cysteine and to participate in Fe–S cluster synthesis. *J. Biol. Chem.*, **271**, 16053–16067.
17. Tong, W.H. and Rouault, T. (2000) Distinct iron–sulfur cluster assembly complexes exist in the cytosol and mitochondria of human cells. *EMBO J.*, **19**, 5692–5700.
18. Tong, W.H., Jameson, G.N., Huynh, B.H. and Rouault, T.A. (2003) Subcellular compartmentalization of human Nfu, an iron–sulfur cluster scaffold protein, and its ability to assemble a [4Fe–4S] cluster. *Proc. Natl Acad. Sci. USA*, **100**, 9762–9767.
19. Barisani, D. and Conte, D. (2002) Transferrin receptor 1 (TfR1) and putative stimulator of Fe transport (SFT) expression in iron deficiency and overload: an overview. *Blood Cells. Mol. Dis.*, **29**, 498–505.
20. Rouault, T.A. and Tong, W.H. (2005) Iron–sulphur cluster biogenesis and mitochondrial iron homeostasis. *Nat. Rev. Mol. Cell. Biol.*, **6**, 345–351.
21. Muhlenhoff, U., Balk, J., Richhardt, N., Kaiser, J.T., Sipos, K., Kispal, G. and Lill, R. (2004) Functional characterization of the eukaryotic cysteine desulfurase Nfs1p from *Saccharomyces cerevisiae*. *J. Biol. Chem.*, **279**, 36906–36915.
22. Biederbick, A., Stehling, O., Rosser, R., Niggemeyer, B., Nakai, Y., Elsasser, H.P. and Lill, R. (2006) Role of human mitochondrial Nfs1 in cytosolic iron–sulfur protein biogenesis and iron regulation. *Mol. Cell. Biol.*, **26**, 5675–5687.
23. Nakai, Y., Nakai, M., Hayashi, H. and Kagamiyama, H. (2001) Nuclear localization of yeast Nfs1p is required for cell survival. *J. Biol. Chem.*, **276**, 8314–8320.
24. Kambampati, R. and Lauhon, C.T. (2000) Evidence for the transfer of sulfane sulfur from IscS to ThiI during the *in vitro* biosynthesis of 4-thiouridine in *Escherichia coli* tRNA. *J. Biol. Chem.*, **275**, 10727–10730.
25. Lauhon, C.T. and Kambampati, R. (2000) The *iscS* gene in *Escherichia coli* is required for the biosynthesis of 4-thiouridine, thiamin, and NAD. *J. Biol. Chem.*, **275**, 20096–20103.
26. Kambampati, R. and Lauhon, C.T. (1999) IscS is a sulfurtransferase for the *in vitro* biosynthesis of 4-thiouridine in *Escherichia coli* tRNA. *Biochemistry*, **38**, 16561–16568.
27. Lukianova, O.A. and David, S.S. (2005) A role for iron–sulfur clusters in DNA repair. *Curr. Opin. Chem. Biol.*, **9**, 145–151.
28. Fan, L., Fuss, J.O., Cheng, Q.J., Arvai, A.S., Hammel, M., Roberts, V.A., Cooper, P.K. and Tainer, J.A. (2008) XPD helicase structures and activities: insights into the cancer and aging phenotypes from XPD mutations. *Cell*, **133**, 789–800.
29. Rudolf, J., Makrantoni, V., Ingledew, W.J., Stark, M.J. and White, M.F. (2006) The DNA repair helicases XPD and FancJ have essential iron–sulfur domains. *Mol. Cell.*, **23**, 801–808.
30. Meyron-Holtz, E.G., Ghosh, M.C. and Rouault, T.A. (2004) Mammalian tissue oxygen levels modulate iron-regulatory protein activities *in vivo*. *Science*, **306**, 2087–2090.